Poole, D., Allen, C., & Rendall, T. (2017). Objective Function and
Constraints for Robust Transonic Aerofoil Optimization. In 58th
AIAA/ASCE/AHS/ASC Structures, Structural Dynamics, and Materials
Conference, Dallas, TX. [AIAA 2017-0360] American Institute of
Aeronautics and Astronautics. DOI: 10.2514/6.2017-0360

Peer reviewed version

Link to published version (if available):
10.2514/6.2017-0360

Link to publication record in Explore Bristol Research
PDF-document

University of Bristol - Explore Bristol Research
General rights

Objective Function and Constraints
for Robust Transonic Aerofoil Optimization

D.J. Poole [*], C.B. Allen [†], T.C.S. Rendall[‡]

Department of Aerospace Engineering, University of Bristol, Bristol, BS8 1TR, U.K.

Construction of the aerodynamic optimization problem is considered within the context of robustness. The most common aerodynamic optimization problem considered is a lift-constrained drag minimization problem (also subject to geometric constraints), however, point-design at transonic flow conditions can produce shock-free solutions and therefore the result is highly localised, where the gains obtained at the design point are outweighed by the losses at off-design conditions. As such, a range optimization problem subject to a constraint on fixed non-dimensional lift with a varying design point is considered to mitigate this issue. It is shown, first from an analytical treatment of the problem, and second from inviscid optimizations, that more robust solutions are obtainable when considering range optimization against drag minimization. Furthermore, to effectively capture the trade-offs that exist in three-dimensional aircraft design between range, lift, drag and speed, it is shown that an induced drag factor is required and this is sufficient to produce optimal solutions exhibiting shocks.

I.   Introduction and Background

A generic single-objective optimization problem optimizes an objective function, J, which is a function of a vector of D design variables, $\boldsymbol{\alpha}$, subject to a set of inequality, $\mathbf{g}$, and equality, $\mathbf{h}$, constraints. Formally, this is written as:

$$\begin{aligned}
\underset{\boldsymbol{\alpha}\in\Re^D}{\text{minimise}} \quad & J(\boldsymbol{\alpha}) \\
\text{subject to} \quad & \mathbf{g}(\boldsymbol{\alpha}) \leq \mathbf{0} \\
& \mathbf{h}(\boldsymbol{\alpha}) = \mathbf{0}
\end{aligned} \tag{1}$$

Aerodynamic shape optimization (ASO) is the process used to optimize a given aerodynamic shape within a computational environment to improve on a design requirement. Numerical simulation methods to model fluid flows are used routinely in industrial design, and increasing computer power has resulted in their integration into the optimization process to produce the ASO framework. The aerodynamic model (normally a computational fluid dynamics (CFD) flow solver) is used to evaluate some metric against which to optimize, which in the case of ASO is an aerodynamic quantity, most commonly drag, subject to a set of constraints which are usually aerodynamic or geometric. Along with the fluid flow model, the ASO framework requires a surface parameterization scheme, which mathematically describes the aerodynamic shape being optimized by a series of design variables. Changes in the design variables, which are made by a numerical optimization algorithm, result in changes in the aerodynamic surface. Numerous advanced optimizations using compressible computational fluid dynamics (CFD) as the aerodynamic model have previously been performed.[1,2,3,4,5] The authors have also presented work in this area, having developed a modularised, generic optimization tool, that is flow solver and mesh type independent, and applicable to any aerodynamic problem.[6,7]

The optimization of the aerodynamic shape to minimize drag is one of the most common optimization problems studied. For typical cruising conditions of a modern transport aircraft, the flow is transonic and

---

*Graduate Student. Email: d.j.poole@bristol.ac.uk

†Professor of Computational Aerodynamics. Email: c.b.allen@bristol.ac.uk

‡Lecturer. Email: thomas.rendall@bristol.ac.uk

American Institute of Aeronautics and Astronautics

the primary source of drag is due to the shock; this causes wave drag and also affects the boundary layer. Eliminating the shock therefore leads to large reductions in the drag of the section, and in inviscid flow, should theoretically lead to a zero drag section. In the first two of a trilogy of papers, Morawetz[8,9] proved that shock-free solutions in inviscid transonic flow around aerofoils were isolated. Due to this result, it was considered difficult, if not impossible to obtain a shock-free aerofoil design. However, the Hodograph method[10,11] allowed shock-free designs to be achieved.[12,13] Harbeck and Jameson[14] later quantified the front in the Mach-C_L space between where shock-free solutions were and were not able to be obtained. Nowadays, shock-free designs for transonic flows around aerofoils are commonly obtained.[15]

A major issue with designing for shock-free solutions is the point-like nature of the design; the off-design performance is often severely compromised for shock-free transonic aerofoils, and can be worse than the initial aerofoil. It was proved in the final paper of the trilogy by Morawetz[16] that shock-free aerofoils in transonic flow would have a shock if the freestream Mach number was perturbed. The flow structure for these types of aerofoils tends to be a single shock for an increase in the freestream Mach number and a double shock for a decrease in the Mach number.[17] Hence, using point-design for aerofoil optimization can be problematic. This issue was also considered when designing the NASA supercritical aerofoils. Harris[18] stated *"permitting a weak shock rather than trying to design for a shock-free design point also reduces the off-design penalties usually associated with point design airfoils"*.

A common way of dealing with this problem is to use multi-point design, where the objective is a combination of the objective at different design points, usually in a weighted sum fashion. Many examples of multi-point design can be found in the literature, see, for example,[19,20,4] or the AIAA Aerodynamic Design Optimization Discussion Group [a] case 4 results.[21,22,23]

Two common issues tend to arise when applying multipoint optimization. The first is that to apply it successfully requires careful selection of both the design points (although these are often known *a priori*), and the weightings between the objectives at those design points. This issue can be eased by using automated weight selections,[24,25] or an integral approach.[26] The second common issue is the cost surrounding multi-point optimization. By the nature of the problem, multipoint design requires a flow solution at each design point per objective function evaluation, which is difficult to avoid. This makes performing high-fidelity multi-point optimization on fine grids prohibitively expensive for more than a handful of design points.

Further issues with multi-point optimization were highlighted in a comprehensive study by Drela.[27] Drela considered single-, two- and four-point optimizations and hypothesised that to avoid point design at each of the considered design points, the number of chosen operating points should be on the order of the number of design variables (this was later validated from a mathematical argument[28]). The problem tends to go back to the proven theory of Morawetz, where, unless there is a shocked solution, a shock will result for a deviation in freestream Mach number, even if multiple points are considered.

The work presented in this paper therefore considers an alternative approach to the construction of the aerodynamic optimization problem, including the choice of design point, design variables, objective function and constraints, for improving both off-design and point design of aerodynamic surfaces without the need for multipoint optimization. Instead of considering drag minimization at a number of design points, the Breguet range parameter, ML/D, is maximised, subject to constant non-dimensional lift. Furthermore, the design point is also considered as a design variable, with Mach number and lift coefficient allowed to vary, however to fully model the trade-offs of speed, lift and drag with range, an induced drag penalty is also introduced. It is shown, both from an analytical treatment and a numerical one, that by considering careful selection of the optimization problem, that good on- and off-design results can be achieved by forcing a shocked solution using an optimization problem that is representative of aircraft design. The advantage of the approach considered in this paper is that the cost is the same as point optimization, and multipoint does not need to be considered.

II. Optimization Framework

In this section, the overall optimization framework used for performing the aerodynamic optimizations outline later is described here. A global optimization approach (as opposed to a gradient-based approach) with a reduced set of design parameters is considered. The geometry and mesh control scheme, optimizer and flow solver are described individually below.

---

[a]<https://info.aiaa.org/tac/ASG/APATC/AeroDesignOpt-DG/default.aspx>

II.A. Shape Control

The geometry and mesh control scheme must be flexible enough to allow sufficient design space investigation and efficient enough to maximise design space coverage with a minimum number of design parameters. The consideration of a global optimization approach necessitates the requirement for a minimum number of design variables to reduce computational burden as much as possible. The design variables used are from a singular value decomposition (SVD) approach,[29] which decomposes a training library of aerofoils into constituent modes and this has the advantage of producing an optimal reduced set of deformation modes according to the optimality theory of SVD.[30]

To determine design variables using an SVD approach, a training library of aerofoils is collated. From this, deformations between all of the aerofoils in the library are calculated to produce a deformation matrix, $\mathbf{\Delta X}$. Performing an SVD then decomposes the deformation matrix into a matrix of mode shapes, $\mathbf{U}$, a matrix of singular values, $\mathbf{\Sigma}$, and a weighting matrix, $\mathbf{V}$, where the decomposition is given by:

$$\mathbf{\Delta X} = \mathbf{U}\mathbf{\Sigma}\mathbf{V}^T \tag{2}$$

The mode shapes, which are the columns of $\mathbf{U}$, are then used as design variables, and in this formulation these are deformative. The method has been shown to produce aerofoil design variables that are effective at inverse shape recovery[31] and aerofoil optimization,[15] requiring as few as six design parameters to obtain optimum solutions in transonic drag minimization cases. The first four design parameters obtained using the SVD method on a library of transonic aerofoils is shown in figure 1 (for visualisation purposes, these are superimposed onto a NACA0012).

(a) Mode 1

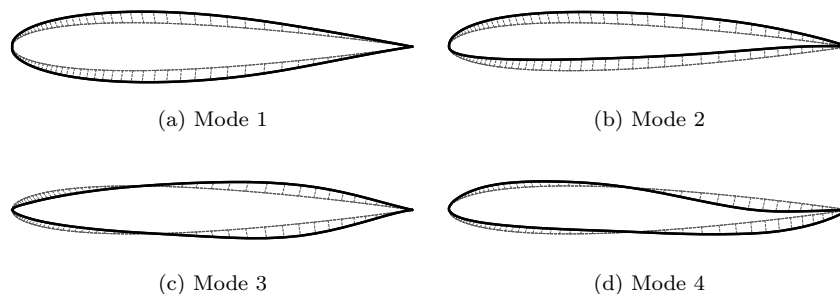(b) Mode 2

(c) Mode 3

(d) Mode 4

Figure 1: Generic aerofoil modes superimposed on NACA0012.

For suitable mesh deformation, an efficient domain element shape parameterization method has been developed by the authors and presented previously for CFD-based shape optimization.[6,32] The parameterization technique, surface control and volume mesh deformation all use radial basis functions (RBFs), wherein global interpolation is used to provide direct control of the design surface and the CFD mesh, which is deformed in a high-quality fashion.[33,34] A small set of control points placed on the aerodynamic surface are deformed using the modal design variables, which subsequently deforms the CFD mesh; this is shown in figure 2 for an exaggerated deformation of the fourth mode.

II.B. Optimizer

A global optimization approach is considered here, as opposed to a gradient-based approach. While global optimization can often be more expensive than performing gradient-based optimization, it is more likely to locate a globally optimal solution in a multimodal design space. The degree of multimodality in the design space of the range optimization with varying design point is unknown, so to avoid any doubt of obtaining global optima, global optimization is performed.

The global optimization algorithm used is an agent-based method, where a population of agents are used to traverse the design space in search of a solution. The location of an agent within the search space of D design variables is $\boldsymbol{\alpha} = [\alpha_1, \alpha_2, \ldots, \alpha_D]^T$, and in an agent-based optimization algorithm moves to a new location at the next iteration of the search by:

$$\boldsymbol{\alpha}(t+1) = \boldsymbol{\alpha}(t) + \mathbf{v}(t) \tag{3}$$

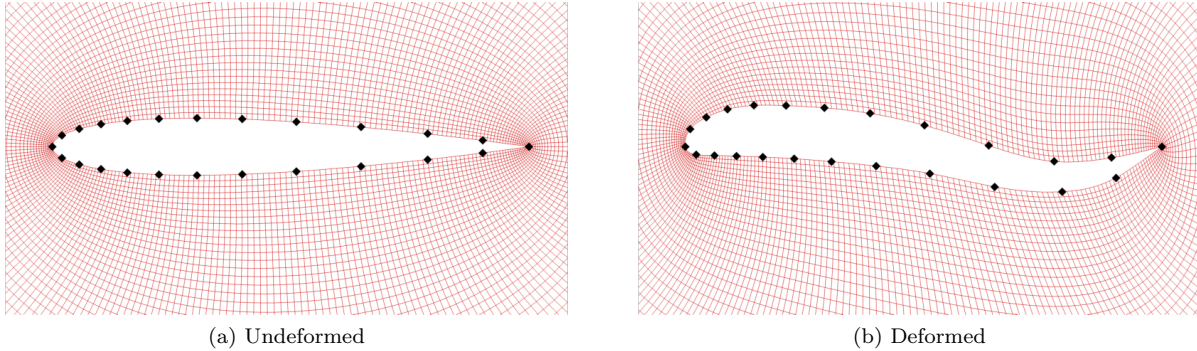(a) Undeformed   (b) Deformed

Figure 2: Exaggerated mesh deformation with mode 4

where $\mathbf{v}$ is the vector of location deformations, which is more commonly termed a particle's velocity, the determination of which separates various agent-based method.

A hybrid of the particle swarm optimization (PSO),[35] and the gravitational search algorithm (GSA)[36] has been developed and used here such that the memory qualities of PSO complement the global transfer of data that occurs in GSA to obtain a highly efficient global search algorithm. Constraints are not directly handled in the PSO or GSA algorithms, hence the separation-sub-swarm (3S)[37] constraint handling method is applied. The 3S method is a constraint handling framework that can be applied to any swarm intelligence algorithm and works by splitting the overall population into two independent swarms every iteration – one swarm containing all of the feasible particles at that iteration (all constraints are satisfied) and one containing all of the infeasible particles at that iteration (at least one constraint is violated). The swarms then independently solve a different objective function, where the objective function of a particle ζ is determined by:

$$\zeta(\boldsymbol{\alpha}) = \begin{cases} J(\boldsymbol{\alpha}) & \text{if } \phi(\boldsymbol{\alpha}) = 0 \\ \phi(\boldsymbol{\alpha}) & \text{else} \end{cases} \tag{4}$$

where ϕ is the sum of the constraint violations. Hence, the infeasible particles have the objective of minimizing the constraint violation and therefore trying to find the feasible region whereas the feasible particles are minimizing the objective that is to be solved for.

The 3S algorithm has been shown to outperform other common constraint handling methods such as penalty methods.[37] The overall framework has also successfully been applied to inviscid and viscous aerofoil optimization.[15]

II.C.   Flow Solver and Meshes

The flow-solver used is a structured multiblock, finite-volume, unsteady, cell-centred scheme solving the compressible Euler or Reynolds-Averaged Navier-Stokes (RANS) equations in cartesian and rotating coordinate system. The convective terms are evaluated using third-order upwind spatial approximation with the flux vector splitting of van Leer.[38] Diffusive terms are evaluated using second-order central differences, and turbulent viscosity is modelled by the Spalart-Allmaras one-equation model.[39,40] Multi-stage Runge-Kutta with local timestepping is used for time integration, and convergence acceleration is achieved through V- and W-cycle multigrid.[41]

Single-block O-meshes were generated for inviscid simulations, using a conformal mapping approach. Figure 3 show views of the 257×97 point meshes, which extend to 100 chords at farfield, of the NACA0012 and RAE2822 aerofoils respectively. All surface cells have an aspect ratio of one.

III.   Consideration of Range Optimization with Varying Design Point

The majority of two-dimensional transonic aerodynamic optimization seeks to minimise drag at a fixed Mach number, with the consequence that aerofoil geometry is modified to force solutions that are shock-free. As noted in the introduction, shock-free design is well known to degrade off-design behaviour at different
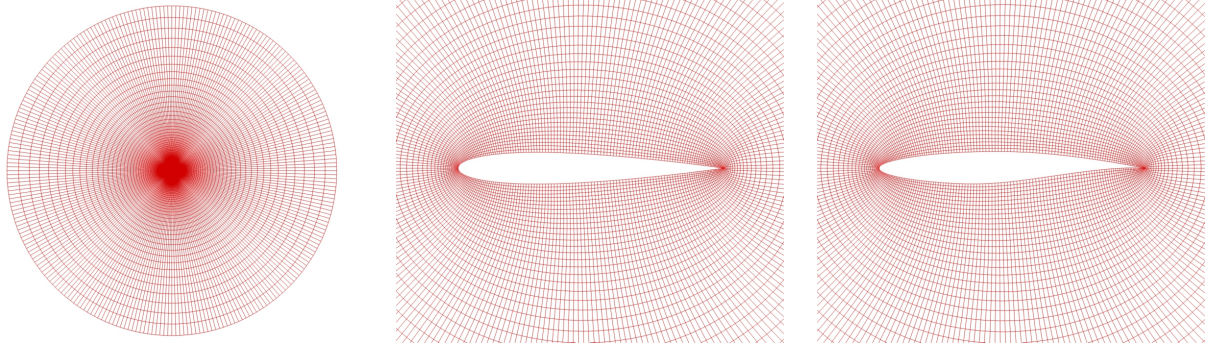
Figure 3: 257×97 NACA0012 and RAE2822 O-meshes

Mach number points, as by Morawetz's proof[16] and Drela's demonstrations;[27] a shock-free solution is strongly local. In addition, aircraft design is not driven purely by drag, and an objective that typifies the industrial process more closely is optimizing the range R, which for a cruising, jet-powered aircraft is given by the Brequet range equation:

$$R = \frac{u}{c}\frac{L}{D}\log\left(\frac{W_1}{W_2}\right) \tag{5}$$

where u is the aircraft velocity, c is the specific fuel consumption (SFC), L and D are the lift and drag, and W_1 and W_2 are the initial and final cruise weights respectively. Under the assumption of constant speed of sound through cruise (so $u \propto M$) and constant SFC, the range factor can be extracted, ML/D, which can be used as the objective function in optimization. The equivalent expression using non-dimensional force coefficients is MC_L/C_D. In this scenario, the aerodynamic optimization problem is enriched with the operating point as a design variable. A similar optimization problem has also be considered by Buckley and Zingg,[26] albeit for low-speed UAV design. The work here expands into inviscid transonic aerofoil design and puts a range optimization problem within the context of robust transonic aircraft design.

Before attempting geometric optimization it is useful to consider the optimization of the operating point of an aerofoil in isolation. A common optimization approach is to constrain C_L, however, this is not suitable in a process where Mach number varies, as equilibrium flight demands a fixed dimensional lift. A more appropriate constraint is therefore $M^2 C_L$, which is a non-dimensional measure of lift ($L = C_L \frac{1}{2}\gamma M^2 PS$). This means that there is only a single free parameter, Mach number, with the aerofoil trimmed to achieve the required lift coefficient for that Mach number. The optimization problem is therefore written as:

$$\begin{aligned}\underset{M}{\text{maximise}} \quad & M\frac{C_L}{C_D}\\ \text{subject to} \quad & M^2 C_L = l\end{aligned} \tag{6}$$

where the lift parameter, l, is some non-dimensional form of lift that must be maintained. In the purely unconstrained problem, where range is maximised with no lift constraint, assuming two dimensional inviscid flow, the solution is known to be the critical Mach number as this is the highest Mach number where there is no wave drag. However, by realistic selection of the lift constraint, a transonic, and shocked solution can be forced.

While it is useful to consider the isolated effect of changing Mach number, the usual aerodynamic optimization process involves modifying some shape to improve the objective. Often this is subject to an internal volume (V) requirement to represent the need to house structure or fuel. Hence, if shape changes are included, defined here by a vector, $\Delta\mathbf{x}$, the full optimization problem is now described as:

$$\begin{aligned}\underset{\Delta\mathbf{x}, M}{\text{maximise}} \quad & M\frac{C_L}{C_D}\\ \text{subject to} \quad & M^2 C_L = l\\ & V \geq V_{initial}\end{aligned} \tag{7}$$

American Institute of Aeronautics and Astronautics

IV. Analytical Treatment for Fixed Shape

Before performing geometric optimization, which is presented later, an analytical treatment is considered, first, for optimizing the problem described by equation 6, to find a value of M that optimizes the Breguet range parameter. This involves differentiating the Breguet range parameter with respect to the design variable, which is Mach number. This is performed by considering inviscid flow, so the only source of drag is due to the shock. An analytical approximation of wave drag is used to approximate the optimal solution.

IV.A. Expression for Optimal Mach

A useful (but approximate) analytical result for wave drag is 'Lock's fourth power rule',[42] which may be used to gain insight in to this problem. The premise for this is that drag per unit height of a normal shock scales with the third power of the Mach number above the critical Mach number, M_c, ie. $M - M_c$, while the shock height is also proportional to $M - M_c$, finally giving a drag proportional to a fourth power. Underpinning assumptions for this result are quite sweeping; Prandtl-Glauert scalings are used for Mach numbers upstream of the shock as well as restrictive forms of C_p moving normal to the aerofoil surface. A calibration constant k also appears in front of the final result to give a final expression for wave drag, C_{D_w}, as:

$$C_{D_w} = k(M - M_c)^4 \qquad (8)$$

Although k can be found through treatment of incompressible data, it is nowadays more straightforward and accurate to use two-dimensional transonic CFD. Lock's work was originally aimed at deriving a measure of compressible aerofoil performance superior to only considering critical Mach number, for which he proposed the use of k, but the Mach-drag scaling remains useful in the transonic regime, where analytical results, however approximate, are relatively rare. The objective here is to apply this in the context of a constrained ML/D operating point.

The physical trade-off for the operating point is very important. At low Mach, lift coefficient must be high. This drives a low critical Mach number and consequently a higher wave drag. At high Mach, the wave drag naturally increases due to the increased offset from M_c. It follows that in between these extremes there lies an optimum where neither the lift coefficient nor Mach number are too high, and it is this optimum that shall be explored with a basic analytical treatment. It is shown that transonic results arise naturally if $M^2 C_L$ is large for the problem given by equation 6 (where the only design variable is Mach number).

The Breguet range parameter is:

$$R = \frac{MC_L}{C_D} \qquad (9)$$

The important factor in this analysis is the wave drag, C_{D_w}, however, C_D is given by the sum of the wave drag and the drag due to other effects, which in this analysis are termed C_{D_0}.

At the optimum solution, the gradient of the objective with respect to the design variable is zero. Using equation 8 and differentiating the objective function with respect to the design variable (M) leads to a fourth power polynomial giving the optimal Mach number for maximum range:

$$F = C_{D_0} + k(M - M_c)^4 + 4Mk(M - M_c)^3 \left(1 - \frac{dM_c}{dM} \right) = 0 \qquad (10)$$

Equation 10 is the resulting polynomial that dictates the optimal condition for the range parameter, and solving allows the optimal Mach number that maximises range to be found. This involves finding M_c and dM_c/dM. The critical Mach number must be differentiated, which is achieved by writing the derivative as:

$$\frac{dM_c}{dM} = \frac{dM_c}{dC_{p_{min}}} \frac{dC_{p_{min}}}{dC_{L_{incomp}}} \frac{dC_{L_{incomp}}}{dM} \qquad (11)$$

where $C_{p_{min}}$ is the minimum pressure coefficient on the aerofoil surface and $C_{L_{incomp}}$ is the incompressible lift coefficient of the aerofoil. The three terms of equation 11 are found through use (and differentiation of) the Prandtl-Glauert scaling and the isentropic flow relation.

Once these terms are evaluated, the solution of equation 10 can be found. It is assumed that the flow is inviscid and in two-dimensions so C_{D_0} can be ignored, and it is also assumed the flow is transonic, so

$M > M_c$ (otherwise C_{D_w} is undefined) meaning there is a positive amount of drag, which is wave drag only, and gives the optimum Mach number, M_{opt}, for maximizing range subject to a constraint on fixed-lift as:

$$M_{opt} = \frac{M_c}{5 - 4\frac{dM_c}{dM}} \qquad (12)$$

To solve this, an outer bisection loop on M_{opt} is used, with M_c found through an inner bisection loop.

IV.B. Results

First, it is interesting to explore the shape of the governing polynomial (equation 10), with the caveat that two-dimensional inviscid flow is considered (meaning $C_{D_0} = 0$) and any roots to the left of M_c are nonsensical. Figure 4 shows the polynomial for NACA 0012 alongside the M_c values; it is important to note that the M_c value plotted corresponds to the M_c value for the rightmost root, therefore, the M_c does not necessarily correspond to a root of the plotted function (this is intrinsic because M_c is a function of M due to the $M^2 C_L$ constraint). Indeed, this is the important point to note from the function shape, because for $l > 0.15$ the root is to the right of M_c, ie. it is transonic. The limit case is also shown, illustrating that, as expected, in this scenario for $l = 0.15$, the optimum Mach number sits just on top of the root of the function, and for any higher value of l the root shifts to the right of M_c and becomes transonic. For any lower value there will be no root to the right of M_c.

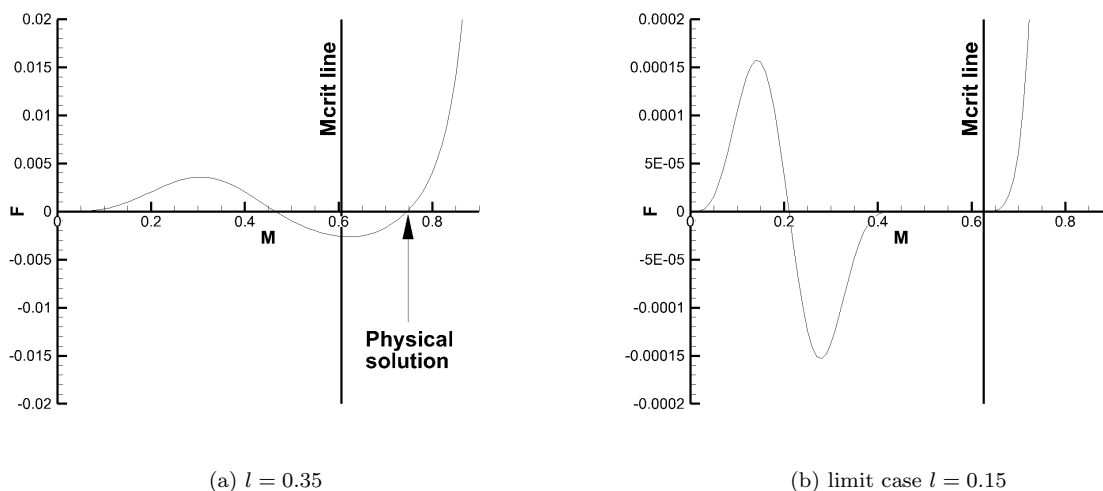(a) $l = 0.35$ (b) limit case $l = 0.15$

Figure 4: Comparison of constraint influence on M_{opt} for NACA 0012

Table 1 shows the M_{opt}/M_c values for varying l for the NACA0012, indicating that the value of 1.23 for $l = 0.35$ compares reasonably to the CFD value of 1.33 (see below), at least to a margin consistent with the assumptions underpinning Lock's relationship. Further, increases in l drive a trend towards a higher M_c, consistent with the root in figure 4 being driven to the right as the function curves increasingly below the axis. Lock's result is limited in accuracy, but it gives a clear indicator of a transonic optimal point in this case (i.e. where $M_{opt}/M_c \geq 1$).

A final interesting point is what value of l necessitates a transonic optimum. This is found from enforcing $M_{opt} = M_c$, which may be done with a bisection loop around the analytical root solver. This reveals that for the NACA 0012 case $l = 0.15$ is the approximate limiting value, while the equivalent value for RAE 2822 is $l = 0.26$. Below these watershed points it is possible to find a subcritical optimal point that satisfies the constraint, whilst above this only a supercritical optimal condition is possible.

IV.C. Numerical Correlation

The primary reason for considering this case is to force a shocked solution, such that point design is avoided. If the $M^2 C_L$ constraint is sufficiently large, at low M it is seen that C_L must rise to compensate, lowering

Table 1: Analytical optimal Breguet Mach numbers as a fraction of M_c for NACA 0012 using $M^2 C_L$ as a constraint

l	M_{opt}/M_c
0.20	1.071
0.25	1.149
0.35	1.23
0.45	1.288
0.55	1.34
0.60	1.366

M_c and increasing wave drag, whilst at high M, increases in M eventually outpace any increase in M_c and wave drag again rises. In between these extremes must lie an optimum, and whether or not it is transonic depends on the value of l that is used. Figure 5 shows sweeps in M computed with inviscid CFD for NACA 0012 and RAE 2822 (each point was trimmed to the appropriate C_L value for that M), illustrating that for NACA 0012 at $l = 0.35$, $M_{opt} = 0.65$ to within the sweep resolution (and since $M_c = 0.49$ for this trim point, $\frac{M}{M_c} = 1.33$, compared to an analytical prediction of 1.23), while for 2822 at $l = 0.45$, $M_{opt} = 0.7$ (and $M_c = 0.55$ so for this trim point, $\frac{M}{M_c} = 1.27$).
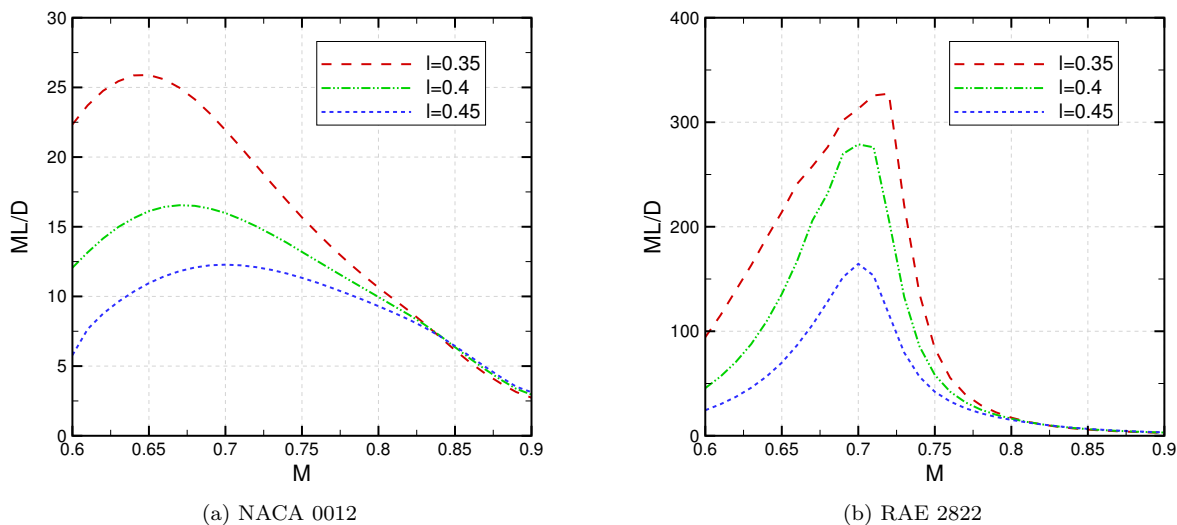

(a) NACA 0012

(b) RAE 2822

Figure 5: Mach sweeps at fixed l showing ML/D

The limited accuracy of the Lock result means that the absolute value of the optimal Mach number differs between the algebraic and the CFD (0.75 versus 0.65 for NACA0012, and 0.8 versus 0.7 for RAE2822) by some margin, but as a fraction of M_c the agreement is surprising. Also, Lock notes[42] an offset in drag rise as a function of Mach of 0.1, which is observable compared to CFD and attributable to the compressible flow simplifications in his analysis, and a similar shift subtracting an increment of 0.1 in optimal Mach number would bring the absolute results much closer to CFD.

V.   Comparison of Approaches for Inviscid Optimization

It has been shown, from an analytical treatment, that the optimum Mach number for the range optimization subject to a fixed non-dimensional measure of lift for a given shape can be supercritical, providing the lift value chosen is above a threshold. It is profound that this result can be shown analytically, and validated

numerically. As such, this approach is suitable for optimization to provide robust off-design performance.

V.A. Single-Point and Multi-Point Optimization

At first, a single-point optimization result is presented on the NACA0012 at a fixed design point to create a baseline result against which to compare. The conventional aerodynamic shape optimization problem of lift-constrained drag minimization at a fixed design point is considered, where the optimization problem is given by:

$$
\begin{aligned}
\underset{\Delta \mathbf{x}}{\text{minimise}} \quad & C_D \\
\text{subject to} \quad & C_L \geq C_{L_{initial}} \\
& V \geq V_{initial}
\end{aligned}
\tag{13}
$$

Second, a multi-point optimization is also presented. The conventional weighted-sum approach, where the overall objective function is a weighted sum of the objective from the individual design points, is considered. A lift constraint on each of the design points is used as well as the volume constraint on the overall shape. For N design points, where each has an objective weighting, $\lambda^{(n)}$, the multi-point optimization problem is therefore given as:

$$
\begin{aligned}
\underset{\Delta \mathbf{x}}{\text{minimise}} \quad & \sum_{n=1}^{N} \lambda^{(n)} C_D^{(n)} \\
\text{subject to} \quad & C_L^{(n)} \geq C_{L_{initial}}^{(n)} \qquad (1 \leq n \leq N) \\
& V \geq V_{initial}
\end{aligned}
\tag{14}
$$

The design variables used for both cases are 12 modal variables (as described in section II.A). It has previously been shown in other work by the authors, that as few as six modal design variables are suitable to obtain shock-free solutions for inviscid optimizations with strong shocks,[15] however, shock-free solutions are more readily obtained with 12 design variables. As such, 12 modal design variables are used for the optimization. The design conditions considered here, for inviscid flow, are:

Condition 1: $M = 0.73$, $C_L = 0.56$

Condition 2: $M = 0.75$, $C_L = 0.56$

A single-point optimization is considered for design condition 2, while a multi-point optimization is considered where the objective function is an equal weighting of the objective functions from each of the two design conditions: $\frac{1}{2}C_D^{(1)} + \frac{1}{2}C_D^{(2)}$.

The optimized results for the single-point optimizations are given in table 2 while the multi-point results are given in table 3. The final drag value of the single-point case at design condition 1 (which is the optimized condition) is slightly lower than the drag value of the multi-point case at the same condition and this is to be expected since the trade-off with the second design condition in the multi-point case restricts, somewhat, the result compared to considering one design point in isolation.

Table 2: Results for single-point inviscid drag minimization

	C_L	C_D	ΔC_D (%)	V
Initial	0.56	0.0234	-	0.081
Optimized	0.56	0.0011	**-95.3%**	0.084

The surface pressure distributions and final surface shapes of the two optimization cases are given in figures 6 and 7 respectively. It is clear that large drag reductions have been obtained and that a shock-free solution has been found for the single-point case, while for the multi-point case a small shock (though these could also be isentropic compressions) results for both flow conditions, albeit at twice the cost of the single-point or range optimizations (presented below). Furthermore, the surface shapes of the two optimizations

Table 3: Results for multi-point inviscid drag minimization

	Condition 1			Condition 2			
	C_L	C_D	ΔC_D (%)	C_L	C_D	ΔC_D (%)	V
Initial	0.56	0.0168	-	0.56	0.0234	-	0.081
Optimized	0.56	0.0012	**-92.9%**	0.56	0.0012	**-94.9%**	0.084

appear remarkably different, indicating that the optimum aerodynamic solution for the single-point compared to the multi-point is substantially different, and this also emphasises the problem with point-design. Both solutions reduce the lift over the forebody of the aerofoil to minimise the leading edge acceleration and therefore avoid a shock forming while the lift is recovered closer to the trailing edge. In specifically the multi-point case, the optimizer was not able to fully eliminate the shocks at the two design conditions, however, the very weak shocks that remain (which could also be isentropic compressions) still pose off-design difficulties.

(a) Single-point
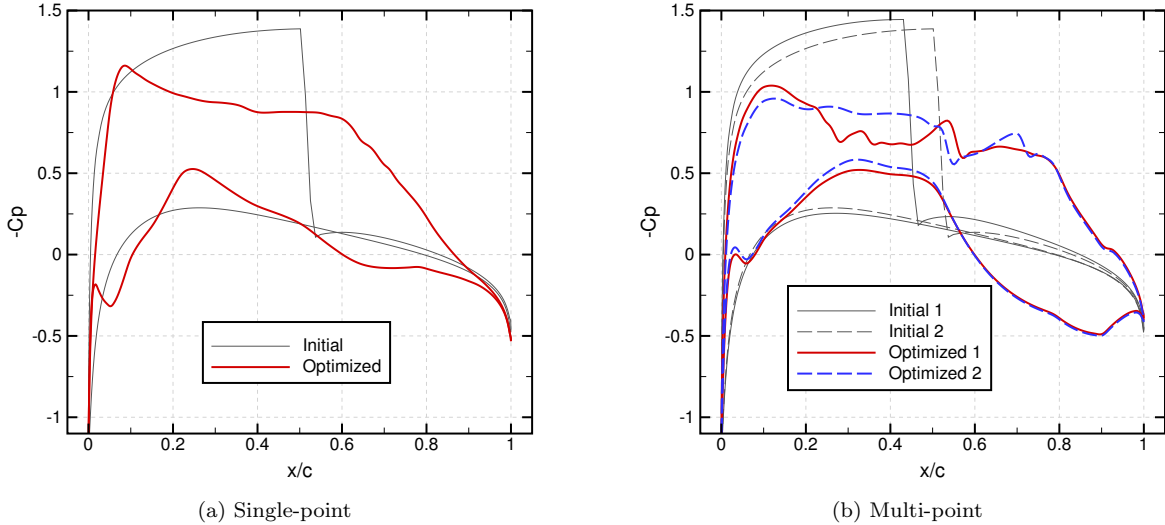
(b) Multi-point

Figure 6: Surface C_P for single-point and multi-point inviscid drag minimizations

V.B. Range Optimization

Range optimizations (the problem described by equation 7) are now presented for the NACA0012 at four different values of lift parameter: $l = 0.35, 0.4, 0.45, 0.5$. However, before progressing, care has to be taken in the construction of the optimization problem. Now that Mach number is a design variable, and also has both a direct (by modifying M, ML/D changes) and indirect (by modifying M, due to the $M^2 C_L$ constraint both lift and drag change and therefore affect the range parameter) influence in the objective function, the true trade-offs in aerodynamic design that occurs due to lift and drag changes need to also be captured. This is only strictly possible in full three-dimensional wing optimization, where induced drag can be captured, however for the aerofoil optimizations considered here, an induced drag factor is added to model these trade-offs and to penalise the negative effect of higher lift coefficients that would exist in three-dimensional wing design.

The objective function is modified to include this induced drag term:
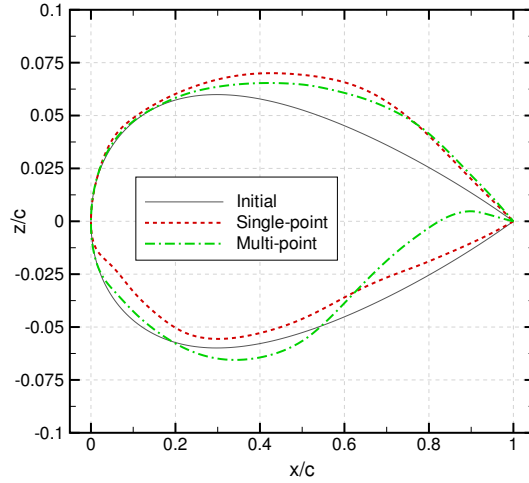
$$C_{D_i} = \kappa C_L^2 \tag{15}$$

Figure 7: Surface shapes for single-point and multi-point inviscid drag minimizations

where κ is the induced drag coefficient, which can be written in terms of the aspect ratio: $\kappa = 1/\pi AR$. The optimization problem now being considered is therefore given by:

$$
\begin{aligned}
\underset{\Delta \mathbf{x}, M}{\text{maximise}} \quad & M \frac{C_L}{C_D + \kappa C_L^2} \\
\text{subject to} \quad & M^2 C_L = l \\
& V \geq V_{initial}
\end{aligned}
\tag{16}
$$

While the effect of adding this factor is to mimic the trade-offs that occur between speed, lift, drag and range, it is interesting to note how this occurs. This factor adds a penalty due to lift to the denominator of the objective function. Hence, a change in the Mach number, which may lead to the shock forming leads to a change in C_L due to the lift constraint. As long as the change in the lift coefficient is greater than the change in the drag coefficient due to the shock, then the shock is permitted. Due to C_L appearing on the numerator and denominator of the objective function, this change will at some point balance out to result in a shocked optimum.

An initial set of optimizations are presented for no induced drag penalty ($\kappa = 0$) to provide a datum. For these optimizations the shape and Mach number are allowed to change with a constraint placed on the internal volume. The optimization results are presented in table 4 and the surface pressure coefficients and surface Mach numbers of the optimized results are shown in figure 8.

Table 4: Results for inviscid range optimizations

l		C_L	C_D	M	ML/D
0.35	Initial	0.56	0.0425	0.800	10.5
	Optimized	0.75	0.0018	0.691	287.9
0.40	Initial	0.63	0.0513	0.800	9.8
	Optimized	0.85	0.0023	0.692	255.7
0.45	Initial	0.71	0.0607	0.800	9.4
	Optimized	0.94	0.0027	0.693	241.3
0.50	Initial	0.79	0.0738	0.800	8.6
	Optimized	1.15	0.0036	0.665	212.4

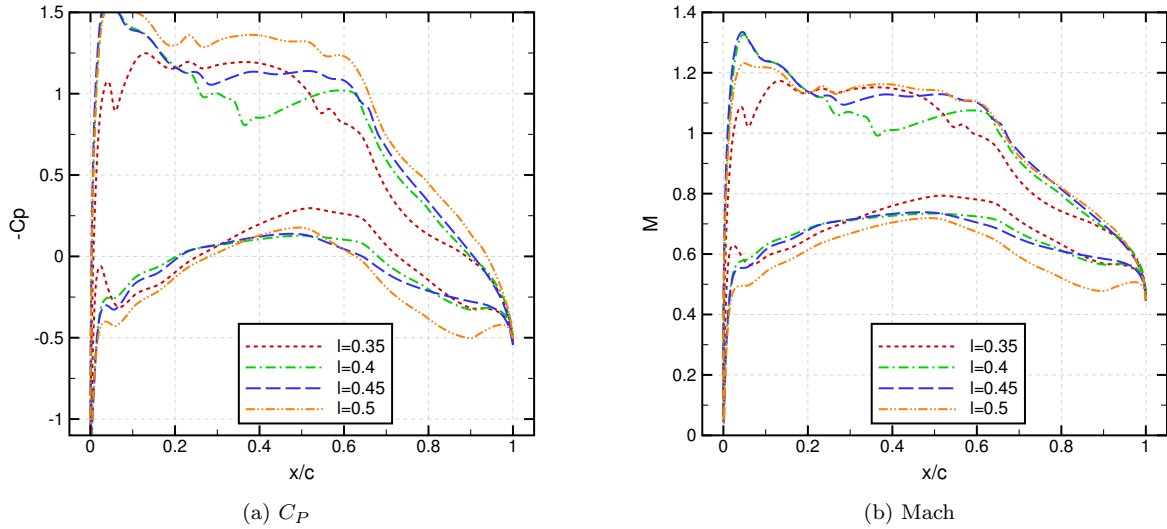American Institute of Aeronautics and Astronautics

Figure 8: Surface C_P and Mach number for inviscid range optimizations

It is clear that the four optimizations have produced shock-free solutions. Furthermore, as was shown in the analytical treatment, higher values of l result in lower optimum range factors, which was also found in the optimization results. However, in the analytical treatment it was also shown that the optimum is supercritical assuming that the lift value chosen is sufficiently high, but this does not necessarily lead to a shocked solution and, in fact, all of the optimizations presented in figure 8 are supercritical (as shown in the surface Mach plot in figure 8), though shock-free. If freestream Mach number was to be increased further, to where a shock forms, then wave drag increases approximately with the fourth power of Mach number, according to Lock.[42] The subsequent increase in objective function due to the increase in Mach number is offset by the reduction in objective function due to the increase in wave drag.

Optimizations for two different values of induced drag penalty (low aspect ratio - $\kappa = 0.1$; high aspect ratio - $\kappa = 0.015$) are now presented. Tables 5 and 6 show the results for these while figure 9 shows the optimized pressure distributions for these optimizations. It is clear that the smaller value of induced drag coefficient (which represents a higher aspect ratio wing) is generally not sufficiently high to ensure the induced drag penalty outpaces the penalty in wave drag due to a shock. The higher value of κ does, however, allow a shocked optimum solution for all four of the l values considered. The general trend in the optimum solution with an increasing value of l is that the optimum Mach number is reasonably similar for the lower values of l but reduces for the very highest l value, and this is a trend seen no matter what the value of induced drag penalty factor. The reduction in the optimal range that would result from a lower Mach number is compensated for by a greater increase in lift coefficient, indicating that any further increase in the Mach number would substantially increase the wave drag due to either, causing a shocked solution in the event of no induced drag penalty, or due to the fourth power rule of Lock.

The final surface shapes of each of these optimizations are shown in figure 10 demonstrating that not only are shocked solutions forced, but that the global form of the surfaces are considerably different depending on the value of κ chosen, while the general form is reasonably independent of the value of l chosen for a fixed κ. It should be noted that small changes in the final shapes of l may have resulted due to a global optimizer being used and that the truly optimum shapes may, in fact, be the same for a fixed κ, where the different l value is obtained by varying the angle of incidence.

When comparing the results from the range optimizations without the induced drag factor to those with it, it is clear that the higher the induced drag penalty is, the lower the optimal lift coefficient and the higher the optimal Mach. This vindicates the use of the induced drag factor, which is a function of lift coefficient, in the objective function to model more closely the real trade-offs that occur in aerodynamic design.

Table 5: Results for inviscid range optimizations with $\kappa = 0.1$ induced drag factor

l		C_L	C_D	C_{D_i}	M	ML/D
0.35	Initial	0.56	0.0425	0.0312	0.800	6.1
	Optimized	0.57	0.0019	0.0326	0.794	13.1
0.40	Initial	0.63	0.0513	0.0401	0.800	5.5
	Optimized	0.65	0.0032	0.0419	0.791	11.3
0.45	Initial	0.71	0.0607	0.0496	0.800	5.2
	Optimized	0.74	0.0037	0.0545	0.782	9.9
0.50	Initial	0.79	0.0738	0.0628	0.800	4.6
	Optimized	0.83	0.0054	0.0696	0.780	8.6

Table 6: Results for inviscid range optimizations with $\kappa = 0.015$ induced drag factor

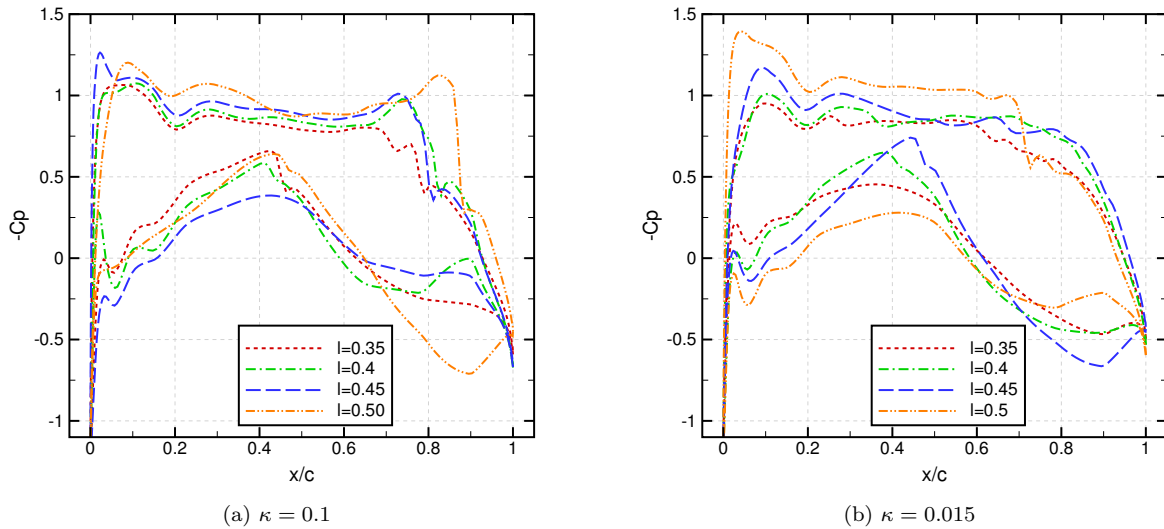| l		C_L	C_D	C_{D_i}	M	ML/D
0.35	Initial	0.56	0.0425	0.0047	0.800	9.5
	Optimized	0.61	0.0013	0.0056	0.766	68.0
0.40	Initial	0.63	0.0513	0.0060	0.800	8.8
	Optimized	0.69	0.0017	0.0071	0.769	60.3
0.45	Initial	0.71	0.0607	0.0076	0.800	8.3
	Optimized	0.77	0.0023	0.0089	0.765	53.0
0.50	Initial	0.79	0.0738	0.0094	0.800	7.6
	Optimized	0.91	0.0031	0.0124	0.747	43.9

(a) $\kappa = 0.1$

(b) $\kappa = 0.015$

Figure 9: Surface C_P for inviscid range optimizations of NACA0012 at different lift values with induced drag penalty
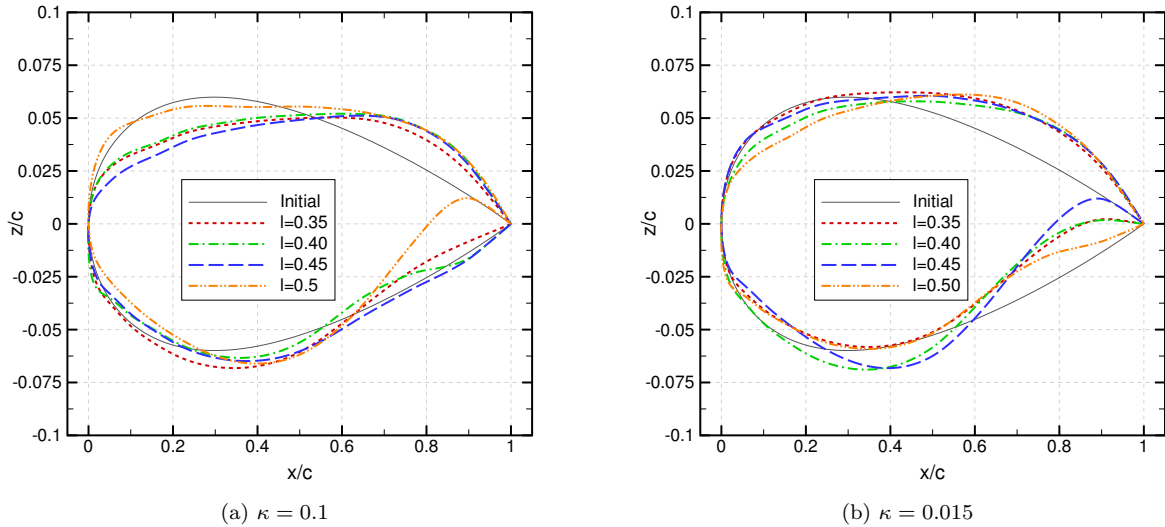
(a) $\kappa = 0.1$

(b) $\kappa = 0.015$

Figure 10: Surface shapes for inviscid range optimizations of NACA0012 at different lift values with induced drag penalty

V.C.   Off-Design Performance

The point of forcing a shocked solution is to mitigate the poor off-design performance that otherwise results from a single-point optimized solution, where, as per the proof of Morowetz,[16] a shock will result from a small perturbation of the freestream conditions from a locally shock-free transonic aerofoil. While multi-point optimization can produce a shocked solution, this is not necessarily always the case and still comes with the multiplication of the cost of evaluating multiple flow solutions per objective function evaluation. However, considering the range-based optimization problem can force a shocked solution. To validate the off-design performance of the results above, namely the single-point, multi-point and range optimizations, sweeps in Mach number are presented for a fixed load (i.e. fixed $M^2 C_L$).

Figures 11 to 14 show Mach sweeps for a fixed loading at $l = 0.35, 0.4, 0.45, 0.5$[b]. The effect on drag and range are shown for the single- and multi-point as well as the range optimized (for $\kappa = 0.1$) for the loading that the sweep is performed at i.e. the range optimized aerofoil in figure 11 is the one optimized for $l = 0.35$, and the one in figure 12 is the one optimized for $l = 0.4$, etc. To allow a fair comparison an induced drag factor has been added to all of the results, which has a coefficient of $\kappa = 0.1$.

First, the effect that fixed loading sweeps have had on the single- and multi-point results demonstrates the poor off-design performance of such optimizations, with the drag coefficient at the design Mach number being upto 200 counts different between the highest and lowest l values, and this is caused entirely by change in lift coefficient required for a fixed load to be maintained. This also means that the drag rise for higher l occurs earlier in the Mach sweep, indicating that a heavier aircraft load would mean a lower cruising Mach number. In general, this poor off-design is the expected result of drag minimization (whether single- or multi-point design is considered). On the other hand, by allowing Mach number to vary in the optimizations and designing for range, the spread in C_D between the different l values at the design point is small. The drag rise occurs considerably later in the Mach sweep, however, more importantly, there is an improvement in the drag value against the baseline aerofoil for all values of Mach in the sweep.

A second, and more indicative measure of optimization performance in this case, is the effect on the range parameter. For all values of l considered, the trend is generally the same, which is that, as expected, the peak range occurs at the Mach number about which the optimization is performed (and in the range optimized cases, where the optimum Mach number is). Also, as to be expected, the range optimized aerofoils have a better range parameter than the drag minimized aerofoils. Despite this, apparently obvious, point, it is interesting to consider the mechanics behind such a result. A drag minimization that takes place about a fixed design point will produce a low drag solution, which increases the range parameter by maximising

---

[b]Note: since Mach number is changing, to ensure a fixed l, C_L is different for each point in the sweep
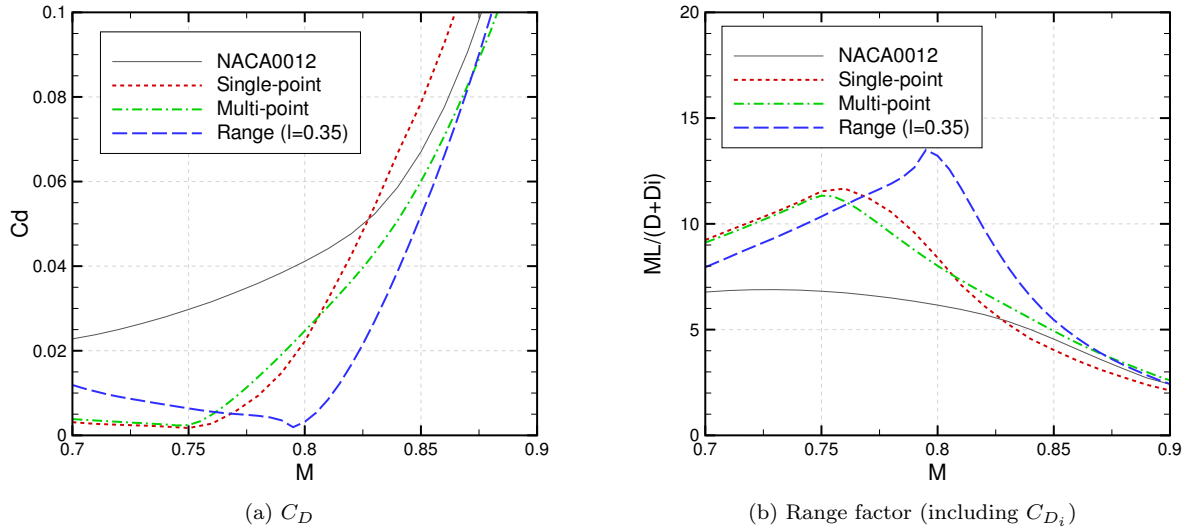
(a) C_D (b) Range factor (including C_{D_i})

Figure 11: Sweep in M for $M^2 C_L = 0.35$ for inviscid optimizations

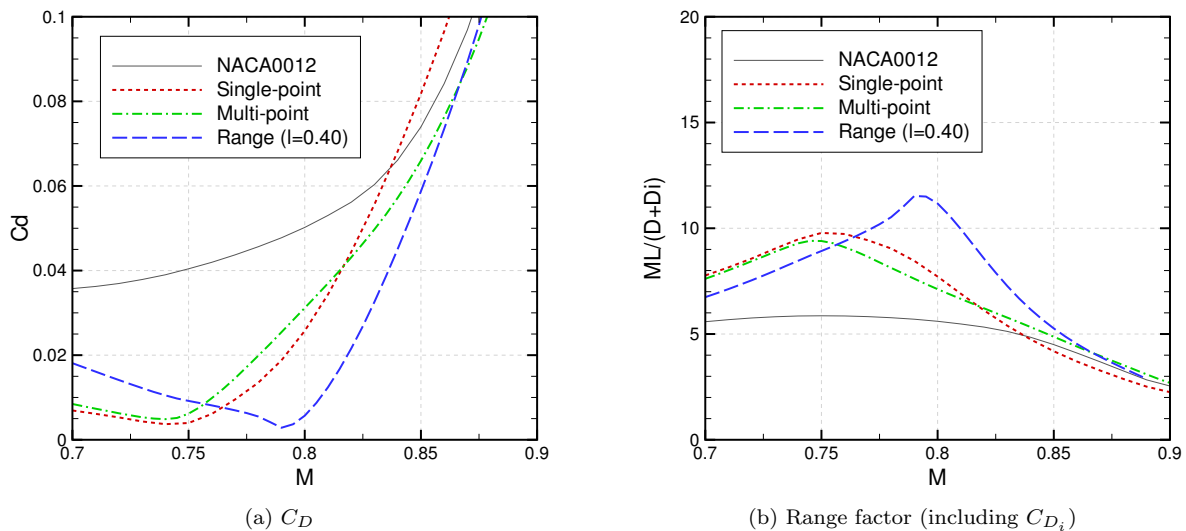(a) C_D (b) Range factor (including C_{D_i})

Figure 12: Sweep in M for $M^2 C_L = 0.40$ for inviscid optimizations

$1/D$. However, by slightly increasing Mach number, which increases ML/D directly, the small drag penalty that also results (and would otherwise force a decrease in ML/D) is outweighed by the increase in velocity resulting in a higher overall range.

Finally, full sweeps are also presented for all of the aerofoils in Mach and l and these are shown in figures 15 and 16, where the contours show the range factor normalised by the maximum range factor in each sweep. The dashed line shows the iso-maximum range (i.e. the Mach number that maximises range for all values of l), which, ideally would be close to vertical meaning that to achieve maximum range, an aicraft could fly at the same Mach number regardless of the load. Hence, it is clear that the original aerofoil (NACA0012) cannot achieve this. On the other hand, The single- and multi-point optimizations show an almost vertical line for this, though at a reasonably low Mach number. This is in contrast to the range optimized aerofoils, which also have close to vertical lines, though at a higher Mach number (this is a similar trend to that seen above, in figures 11 to 14).
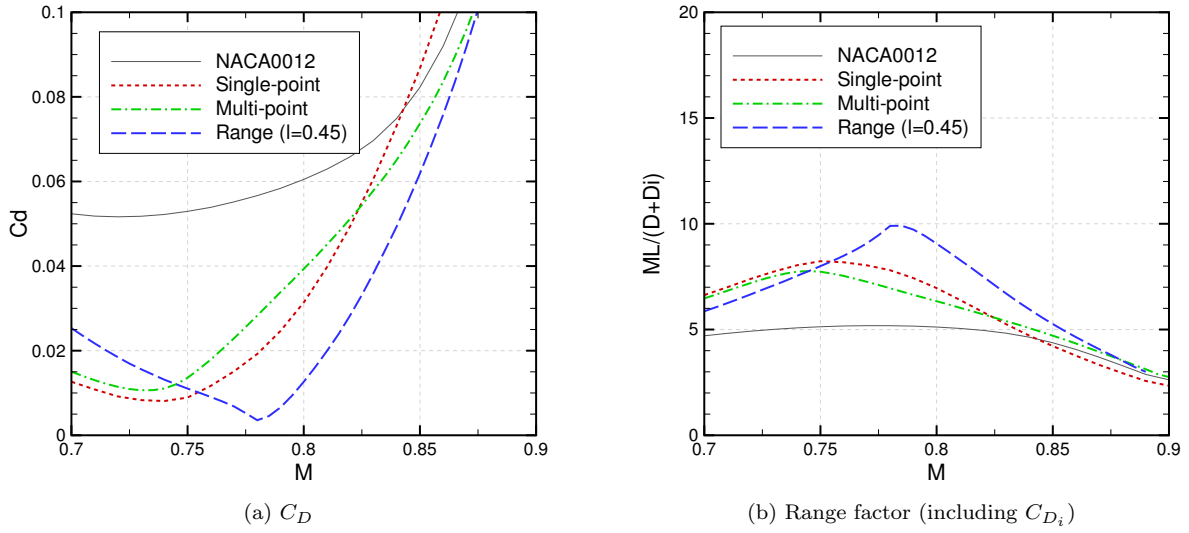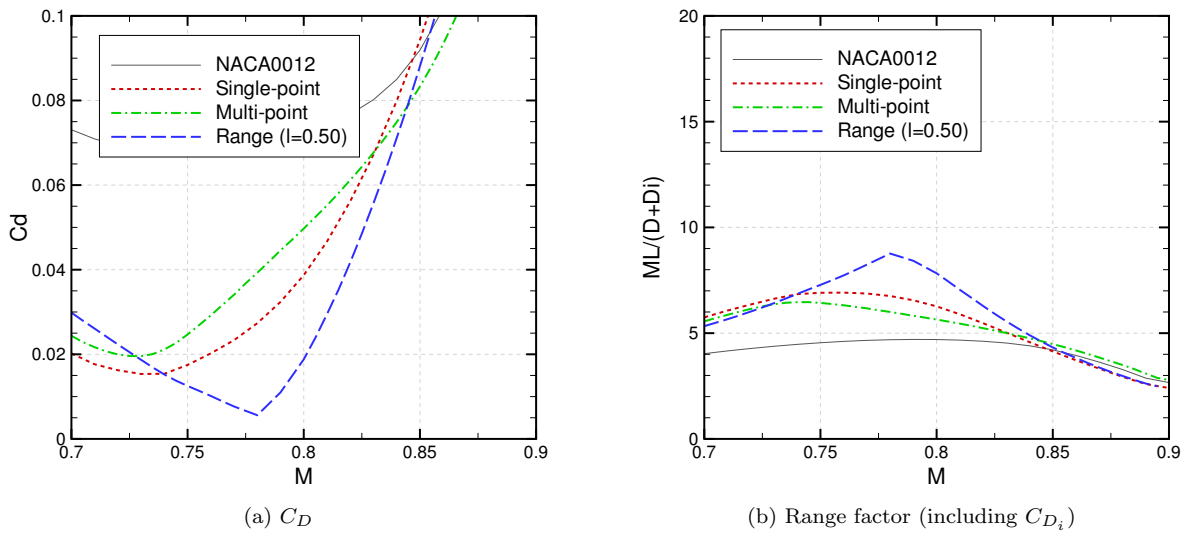
(a) C_D

(b) Range factor (including C_{D_i})

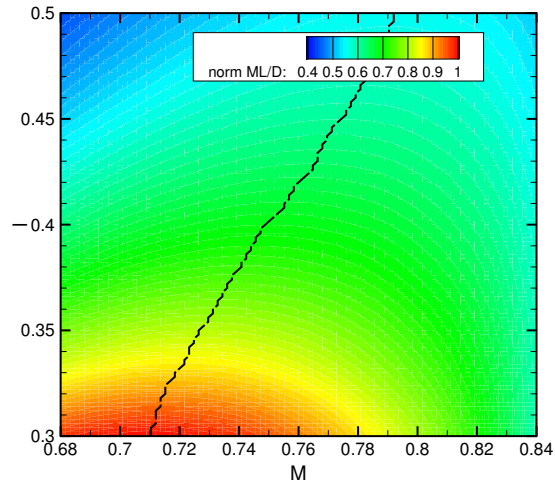Figure 13: Sweep in M for $M^2 C_L = 0.45$ for inviscid optimizations

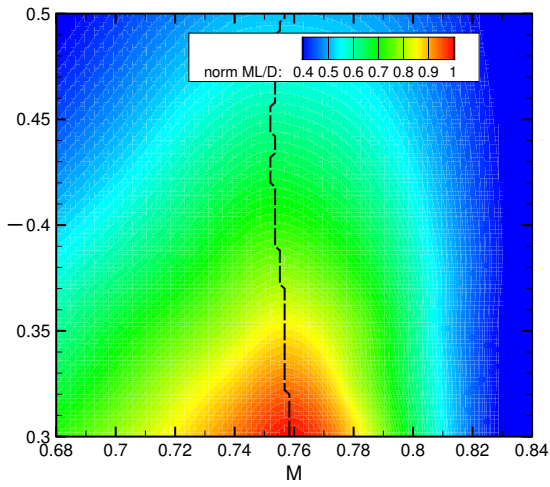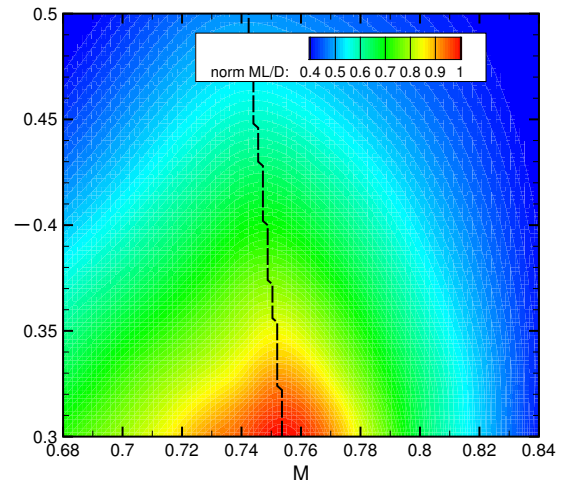(a) C_D

(b) Range factor (including C_{D_i})

Figure 14: Sweep in M for $M^2 C_L = 0.50$ for inviscid optimizations

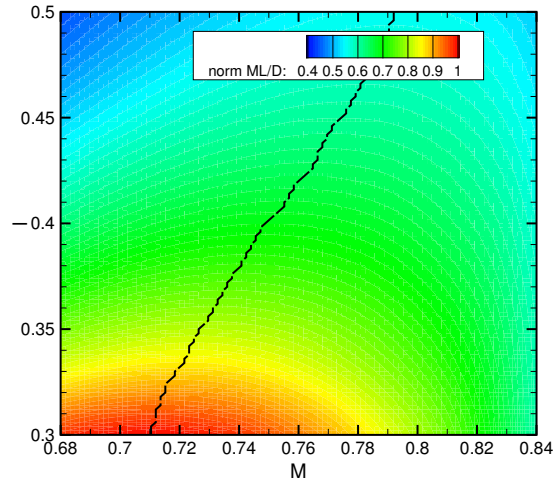American Institute of Aeronautics and Astronautics
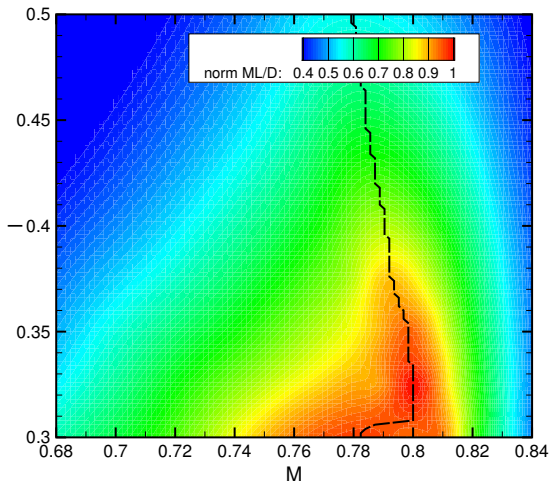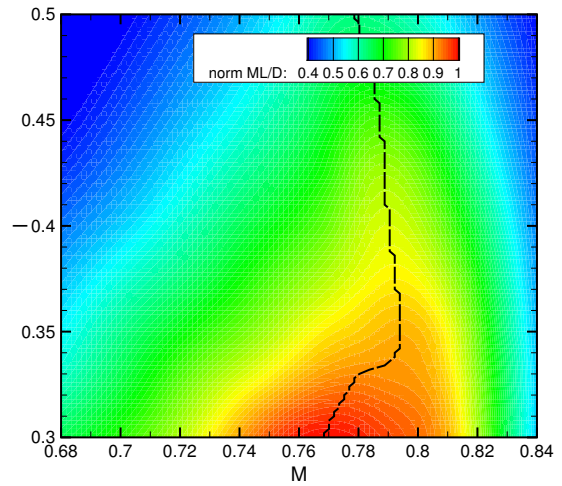
(a) NACA0012

(b) Single-point

(c) Multi-point

Figure 15: Contours in range factor (including C_{D_i}) for inviscid drag optimizations (maximum range line highlighted)
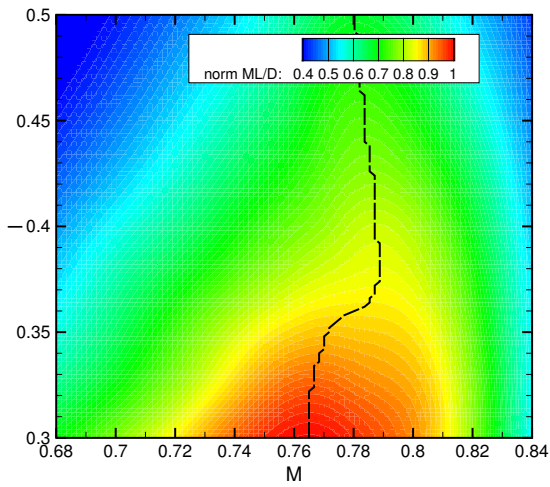
(a) NACA0012

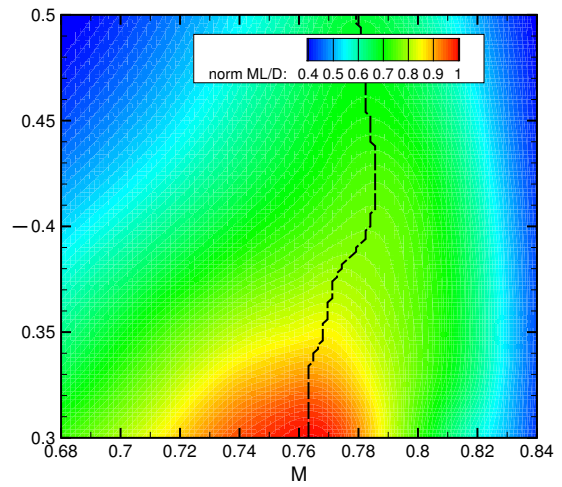(b) Range ($l = 0.35$)

(c) Range ($l = 0.40$)

(d) Range ($l = 0.45$)

(e) Range ($l = 0.50$)

Figure 16: Contours in range factor (including C_{D_i}) for inviscid range optimizations (maximum range line highlighted)

American Institute of Aeronautics and Astronautics

VI.   Conclusions

A consideration of the choice of objective function and constraints has been presented. A problem in single-point designed aerodynamic shapes is that the off-design performance of point design aerofoils can be severely degraded. Multi-point optimization can alleviate this to a certain extent, though at the expense of computing extra flow solutions for each objective function leading to large cost multipliers. Considering the Breguet range parameter has therefore been considered with the design point also being a variable. The Mach number is allowed to vary, hence a non-dimensional measure of lift needs to be introduced as a constraint.

An analytical treatment has been presented where the optimization problem has been differentiated using an approximation for the wave drag to yield the optimal Mach number for a given aerodynamic shape for this design problem. This correlates well with CFD predictions. The insight from the analytical treatment demonstrates that the optimal solution is supercritical if the specified lift is over a given limit for a given shape.

Inviscid range optimizations have also been performed with varying shape using a global optimization framework. To mimic, more closely, the real trade-offs that exist in aircraft design between Mach number, lift, drag and range, an induced drag factor has been added to the optimization problem and this is essential in the range problem since the trade-off in maximising range by minimizing drag due to minimizing Mach number need to be set against the increase in induced drag that occur due to the necessary increase in lift coefficient in this case. It has been shown that a shocked, and more robust, optimal solution can be found when performing range optimization, indicating that this may be a suitable optimization problem to consider in the context of robustness.

References

[1] Hicks, R. M. and Henne, P. A., "Wing Design by Numerical Optimization," *Journal of Aircraft*, Vol. 15, No. 7, 1978, pp. 407–412.

[2] Qin, N., Vavalle, A., Le Moigne, A., Laban, M., Hackett, K., and Weinerfelt, P., "Aerodynamic Considerations of Blended Wing Body Aircraft," *Progress in Aerospace Sciences*, Vol. 40, No. 6, 2004, pp. 321–343.

[3] Nielsen, E. J., Lee-Rausch, E. M., and Jones, W. T., "Adjoint Based Design of Rotors in a Noninertial Frame," *Journal of Aircraft*, Vol. 47, No. 2, 2010, pp. 638–646.

[4] Lyu, Z., Kenway, G. K. W., and Martins, J. R. R. A., "Aerodynamic Shape Optimization Investigations of the Common Research Model Wing Benchmark," *AIAA Journal*, Vol. 53, No. 4, 2015, pp. 968–985.

[5] Choi, S., Lee, K. H., Potsdam, M., and Alonso, J. J., "Helicopter Rotor Design Using a Time-Spectral and Adjoint Based Method," *Journal of Aircraft*, Vol. 51, No. 2, 2014, pp. 412–423.

[6] Morris, A. M., Allen, C. B., and Rendall, T. C. S., "CFD-based Optimization of Aerofoils Using Radial Basis Functions for Domain Element Parameterization and Mesh Deformation," *International Journal for Numerical Methods in Fluids*, Vol. 58, No. 8, 2008, pp. 827–860.

[7] Allen, C. B. and Rendall, T. C. S., "Computational-Fluid-Dynamics-Based Optimisation of Hovering Rotors Using Radial Basis Functions for Shape Parameterisation and Mesh Deformation," *Optimization and Engineering*, Vol. 14, 2013, pp. 97–118.

[8] Morawetz, C. S., "On the non-existence of continuous transonic flows past profiles I," *Communications on Pure and Applied Mathematics*, Vol. 9, No. 1, 1956, pp. 45–68.

[9] Morawetz, C. S., "On the non-existence of continuous transonic flows past profiles II," *Communications on Pure and Applied Mathematics*, Vol. 10, No. 1, 1957, pp. 107–131.

[10] Garabedian, P. R. and Korn, D. G., "Analysis of Transonic Airfoils," *Communications on Pure and Applied Mathematics*, Vol. 24, No. 6, 1971, pp. 841–851.

[11] Bauer, F., Garabedian, P., and Korn, D. G., "A Theory of Supercritical Wing Sections, with Computer Programs and Examples," *Lecture Notes in Economics and Mathematical Systems*, 1972.

[12] Boerstoel, J., "A Survey of Symmetrical Transonic Potential Flows around Quasi-elliptical Aerofoil Sections," Tech. rep., NLR, 1967, NLR Report TR.T179.

[13] Nieuwland, G., "Transonic Potential Flow around a Family of Quasi-elliptical Aerofoil Sections," Tech. rep., NLR, 1967, NLR Report TR.T172.

[14] Harbeck, M. and Jameson, A., "Exploring the Limits of Transonic Shock-free Airfoil Design," *43rd AIAA Aerospace Sciences Meeting and Exhibit*, Reno, Nevada, 2005, AIAA Paper 2005-1041.

[15] Poole, D. J., Allen, C. B., and Rendall, T. C. S., "High-fidelity aerodynamic shape optimization using efficient orthogonal modal design variables with a constrained global optimizer," *Computers & Fluids*, Vol. 143, 2017, pp. 1–15.

[16] Morawetz, C. S., "On the non-existence of continuous transonic flows past profiles III," *Communications on Pure and Applied Mathematics*, Vol. 11, No. 1, 1958, pp. 129–144.

[17] Jameson, A., Vassberg, J. C., and Ou, K., "Further Studies of Airfoils Supporting Non-Unique Solutions in Transonic Flow," *AIAA Journal*, Vol. 50, No. 12, 2012, pp. 2865–2881.

[18] Harris, C. D., "NASA Supercritical Aerofoils," Tech. rep., Langley Research Center, Hampton, Virginia, March 1990, NASA Technical Paper 2969.

[19]Epstein, B., Jameson, A., Peigin, S., Roman, D., Harrison, N., and Vassberg, J., "Comparative Study of Three-Dimensional Wing Drag Minimization by Different Optimization Techniques," *Journal of Aircraft*, Vol. 46, No. 2, 2009, pp. 526–541.

[20]Buckley, H. P., Zhou, B. Y., and Zingg, D. W., "Airfoil Optimization Using Practical Aerodynamic Design Requirements," *Journal of Aircraft*, Vol. 47, No. 5, 2010, pp. 1707–1719.

[21]Meheut, M., Destarac, D., Carrier, G., Anderson, G., Nadarajah, S., Poole, D., Vassberg, J., and Zingg, D., "Gradient-Based Single and Multi-points Aerodynamic Optimizations with the elsA Software," *53rd AIAA Aerospace Sciences Meeting*, Kissimmee, Florida, 2015, AIAA Paper 2015-0263.

[22]Kenway, G. K. W. and Martins, J. R. R. A., "Multipoint Aerodynamic Shape Optimization Investigations of the Common Research Model Wing," *53rd AIAA Aerospace Sciences Meeting*, Kissimmee, Florida, 2015, AIAA Paper 2015-0264.

[23]LeDoux, S. T., Vassberg, J. C., Young, D. P., Fugal, S., Kamenetskiy, D., Huffman, W. P., Melvin, R. G., and Smith, M. F., "Study Based on the AIAA Aerodynamic Design Optimization Discussion Group Test Cases," *AIAA Journal*, Vol. 53, No. 7, 2015, pp. 1910–1935.

[24]Zingg, D. W. and Elias, S., "Aerodynamic Optimization Under a Range of Operating Conditions," *AIAA Journal*, Vol. 44, No. 11, 2006, pp. 2787–2792.

[25]Liem, R. P., Kenway, G. K. W., and Martins, J. R. R. A., "Multimission Aircraft Fuel-Burn Minimization via Multipoint Aerostructural Optimization," *AIAA Journal*, Vol. 53, No. 1, 2015.

[26]Buckley, H. P. and Zingg, D. W., "Approach to Aerodynamic Design Through Numerical Optimization," *AIAA Journal*, Vol. 51, No. 8, 2013, pp. 1972–1981.

[27]Drela, M., "Pros and Cons of Airfoil Optimization," *Frontiers of Computational Fluid Dynamics*, edited by D. Caughey and M. Hafez, World Scientific, 1998, pp. 363–381.

[28]Li, W., Huyse, L. W., and Padula, S., "Robust airfoil optimization to achieve drag reduction over a range of Mach numbers," *Structural and Multidisciplinary Optimization*, Vol. 24, No. 1, 2002, pp. 38–50.

[29]Poole, D. J., Allen, C. B., and Rendall, T. C. S., "Metric-Based Mathematical Derivation of Efficient Airfoil Design Variables," *AIAA Journal*, Vol. 53, No. 5, 2015, pp. 1349–1361.

[30]Eckart, C. and Young, G., "The Approximation of One Matrix by Another of Lower Rank," *Psychometrika*, Vol. 1, No. 3, 1936, pp. 211–218.

[31]Masters, D. A., Taylor, N. J., Rendall, T. C. S., Allen, C. B., and Poole, D. J., "A Geometric Comparison of Aerofoil Shape Parameterisation Methods," *54th AIAA Aerospace Sciences Meeting*, San Diego, California, 2016, AIAA Paper 2016-0558.

[32]Morris, A. M., Allen, C. B., and Rendall, T. C. S., "Domain-Element Method for Aerodynamic Shape Optimization Applied to a Modern Transport Wing," *AIAA Journal*, Vol. 47, No. 7, 2009, pp. 1647–1659.

[33]Rendall, T. C. S. and Allen, C. B., "Unified Fluid-Structure Interpolation and Mesh Motion Using Radial Basis Functions," *International Journal for Numerical Methods in Engineering*, Vol. 74, No. 10, 2008, pp. 1519–1559.

[34]Rendall, T. C. S. and Allen, C. B., "Efficient Mesh Motion Using Radial Basis Functions with Data Reduction Algorithms," *Journal of Computational Physics*, Vol. 228, No. 17, 2009, pp. 6231–6249.

[35]Kennedy, J. and Eberhart, R., "Particle Swarm Optimization," *1995 IEEE International Conference on Neural Networks*, Perth, Australia, 1995.

[36]Rashedi, E., Nezamabadi-pour, H., and Saryazdi, S., "GSA: A Gravitational Search Algorithm," *Information Sciences*, Vol. 179, 2009, pp. 2232–2248.

[37]Poole, D. J., Allen, C. B., and Rendall, T. C. S., "A Generic Framework for Handling Constraints with Agent-Based Optimization Algorithms and Application to Aerodynamic Design," *Optimization and Engineering*, 2016, Published online.

[38]van Leer, B., "Flux-vector splitting for the Euler equations," *Eighth International Conference on Numerical Methods in Fluid Dynamics*, Lecture Notes in Physics, 1982, pp. 507–512.

[39]Spalart, P. R. and Allmaras, S. R., "A One-Equation Turbulence Model for Aerodynamic Flows," *Recherche Aérospatiale*, Vol. 1, 1994, pp. 5–21.

[40]Allmaras, S. R., Johnson, F. T., and Spalart, P. R., "Modifications and Clarifications for the Implementation of the Spalart-Allmaras Turbulence Model," *Seventh International Conference on Computational Fluid Dynamics (ICCFD7)*, Big Island, Hawaii, 2012, Paper ICCFD7-1902.

[41]Allen, C. B., "Multigrid Convergence of Inviscid Fixed- and Rotary-Wing Flows," *International Journal for Numerical Methods in Fluids*, Vol. 39, No. 2, 2002, pp. 121–140.

[42]Lock, C. N. H., "The Ideal Drag Due to a Shock Wave Parts I and II," Tech. rep., Aeronautical Research Council, 1951, ARC report 2512.